A Preliminary Study On The Inclination And Shape Of Jets Issuing From An Orifice In The Lateral Wall Of A Pipe

Simone Ferrari[1,*], *Luca* Salvadori[1], *Michela* Garau[1], and *Giorgio* Querzoli[1]

[1]DICAAR – Dip. Ingegneria Civile, Ambientale e Architettura, University of Cagliari, via Marengo 2, 09123 Cagliari, Italy

Abstract. The topic of the behaviour of jets issuing from an orifice in the lateral wall of a pipe is of interest in many engineering fields, such as sea discharges of pollutants via submerged pipes, diffusers to mix different fluids in tanks and reactors, leakage in industrial and civil pipelines, etc. Most of the previous researches focuses on the pressure loss across the orifice, without taking into account the modification of the internal flow and, most important, the direction and shape of the jet issuing from the outlet: as a matter of fact, this is usually considered perpendicular to the axis of the pipe and axisymmetric. We have investigated these issues in the laboratory via Digital Image Analysis techniques, namely LIF (Laser Induced Fluorescence) to measure concentration fields and FTV (Feature Tracking Velocimetry) to measure velocity fields, varying the ratio of the flow rate of the jet to the flow rate in the pipe before the orifice. Here we present some preliminary results, highlighting how the jet is not always perpendicular to the axis of the pipe nor axisymmetric: the inclination increases and the axisymmetry decreases when the ratio of the flow rates above described decreases.

1 Introduction

A jet issuing from the lateral wall of a pipe where a fluid is flowing can be used to discharge a pollutant in a fluid receiving body, to mix a fluid into another fluid in a tank, a reactor or a reservoir, or can be the unwanted consequence of a failure of the wall material, with a consequent fracture and leak.

The first case is the one, for instance, of marine outfall via submerged pipes, where a common configuration for the diffusers is the use of orifices in the lateral wall of a submerged outfall pipe (see, for instance, Missimer et al. 2015 [1], Ferrari and Querzoli, 2010 [2], Avanzini 2006 [3], Wood 1993 [4]). The topic of the behavior of the jet issuing from an orifice in the lateral wall of the outfall pipe is even more relevant when multi-port diffusers are employed, as the jets are usually considered as perpendicular to the pipe axis and axisymmetric (Wue et al., 2014 [5], Al-Ghamdi 2010 [6]). The second case is the one, for instance, of the diffusers adopted to mix different fluids in a tanks or reactors. One example is can be find in Photobioreactors (PBRs) and chemical reactors (in order to drive completely developed chemical reactions or to realize industrial products, Anderson et al., 2014 [7]). Another example is the diffuser optimization to reduce the thermal stratification in the tanks used for thermal energy storage (TES), in order to reduce costs and energy consumption in the air conditioning systems of large buildings (Osman et al. 2008 [8]).The third case, the accidental leak jets generating from a fracture in the wall of a pipeline (as a leak from a fracture in a pipeline can be considered as a leak from an orifice, van Zyl, 2014 [9]), has received a particular attention during the last years. In fact, the new scenarios related to the availability and cost of water, oil and gas and of their transportation have forced to pay more attention to the efficiency of the distribution systems and, in particular, to the leakage control and detection (Soleimani nia et al., 2019 [10], Ferrante et al., 2013) [11]). Moreover, a high-pressure non-controlled jet can be dangerous for the safety of people working or living in the vicinity of industrial plants and pipelines (Mohsin et al., 2015 [12]).

Most of the previous researches focus on the pressure drop across the orifice or fracture in the flow direction, via numerical simulations (Cassa et al, 2010 [13]), laboratory experiments (van Zyl and Clayton, 2007 [14]) or theoretical studies (van Zyl, 2014 [9]). Other Authors investigated the jet behaviour outside the pipe of reacting or flammable fluids, such as the release of hydrogen or helium into the air, with the buoyancy (i.e. the difference in density) and the chemical reactions playing a relevant role in the behaviour of the jet (Soleimani nia et al., 2018 [15] and 2019 [10]). Anyway, they concluded that the conventional round jet assumptions are not adequate to predict the behavior of turbulent buoyant jets issuing from a slot on the lateral wall of a pipe, in particular regarding the direction and axisymmetry of the jets.

Here we focus on the behavior (in particular, shape and direction) of non-buoyant or simple jets, issuing from a sharp-edged orifice on the lateral wall of pipe, released into a fluid with the same density. The employment of a sharp-edged orifice derives from the fact that previous investigations on simple jets have measured that the mixing efficiency is higher in sharp-edged orifice jets than

* Corresponding author: ferraris@unica.it

in jets released in other ways, such from contoured nozzles or at the end of a pipe (Hashiehbaf and Romano (2013) [16], Mi et al. 2001 [17]). Moreover, as stated in Mi et al., 2007 [18], this configuration is widely used in many engineering field.

We have performed some experimental campaigns in the Hydraulics Laboratory of the DICAAR – University f Cagliari (Italy), measuring via Digital Image Analysis techniques both concentration and velocity fields, inside and outside the pipe in the region close to the orifice. In the present work, we will show some preliminary results regarding the concentration measurements.

2 Physical parameters

A simple jet is the release, with a non-negligible initial momentum, of a fluid into a fluid with the same density. A buoyant jet is a jet released into a fluid with a different density. Therefore, if a fluid jet is released into the air, like in the case of oil or water pipelines, a buoyant jet will develop, whilst if a water jet is released into water, a simple jet will develop, like in the present case.

Regarding the shape, a jet can be usually classified as round or axisymmetric, when the orifice it is released from is circular; as two-dimensional, when the orifice is a line; as three-dimensional, when the orifice has a non-circular shape (Hashiehbaf and Romano, 2013 [16]). In the present case, the jet is released from a sharp-edged round orifice.

The key non-dimensional number governing the flow regime is the ratio of the inertial force to the viscous force, the Reynolds number *Re*: if *Re* is larger than a critical value, the flow is turbulent. In the present case, there are three relevant *Re*: a jet Reynolds number Re_J, a pipe Reynolds number Re_P and a backward step Reynolds number Re_h.

The jet Reynolds number is defined as:

$$Re_J = \frac{U_J D_J}{\upsilon} \qquad (1)$$

where U_J is the jet mean velocity at the orifice, D_J the diameter of the orifice (0.08 m) and υ the kinematic viscosity of the released fluid (tap water). The critical value of Re_J has been measured as 500.

The pipe Reynolds number is defined as:

$$Re_P = \frac{U_P D_P}{\upsilon} \qquad (2)$$

where U_P is the mean velocity in the pipe before the orifice, D_P the internal diameter of the pipe (0.064 m).

The backward step Reynolds number is defined as:

$$Re_h = \frac{U_h h}{\upsilon} \qquad (3)$$

where U_h is the mean velocity in the pipe before the divergent reach and h is the step height (0.019 m).

The distance of flow reattachment after the backward step is X_d.

In the case of buoyant jets, another relevant non-dimensional number is the Richardson number *Ri*, that is the ratio of gravitational force to inertial force (the opposite is called the densimetric Froude number). In the present case, *Ri* is null, as the jet and the receiving body have the same density.

The flow rate in the pipe before the orifice (Figure 1) is Q_1, the flow rate after the orifice Q_2, the flow rate of the jet through the orifice is Q_3, and the ratio of the flow rate of the jet to the flow rate before the orifice is r:

$$r = \frac{Q_3}{Q_1} \qquad (4)$$

The angle between the jet axis and the line perpendicular to the pipe axis is θ.

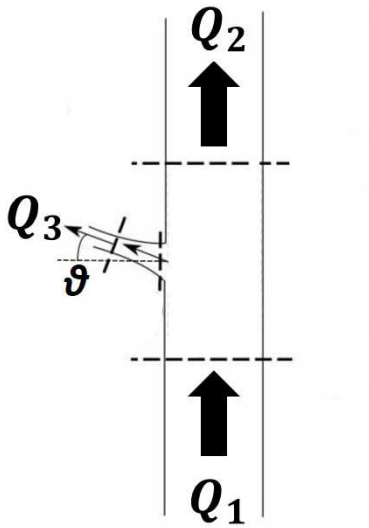

Fig. 1. Definition of the three flow rates in the pipe: Q_1 is the flow rate in the pipe before the orifice, Q_2 the flow rate in the pipe after the orifice, Q_3 the flow rate of the jet.

3 Experimental set-up and data acquisition and elaboration

The jet is released from a sharp-edged round orifice (with a diameter D_J of 8.0 mm) on the lateral wall of a pipe of transparent Perspex (with an internal diameter D_P of 64.0 mm) with a length of 600.0 mm and with a divergent reach at its beginning and a convergent reach at its end (Figure 2).

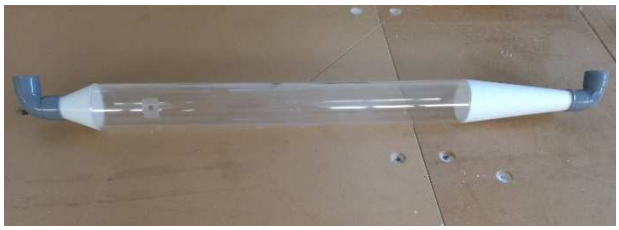

Fig. 2. Pipe with the sharp edged orifice, the divergent reach and the convergent reach; flow from right to left.

Divergent and convergent reaches are needed to connect the Perspex pipe to a rubber pipe (with a diameter of 25.4 mm) that, in turns, are connected to a constant-

head closed-loop hydraulic circuit. The divergent has a length of 185.0 mm and its wall has an inclination of around 6°, in order to minimize the flow separation. As a matter of fact, following Westphal et al (1984) [19], the divergent reach is long enough to allow the flow reattachment with Re_h higher than $1 \cdot 10^3$, that is with velocity in the pipe U_h higher than 0.05 ms^{-1} (Figure 3). In the experiments presented hereafter, U_h was around 0.1 ms^{-1} and U_P was around 0.1 ms^{-1}, corresponding to a $Re_h \approx 12 \cdot 10^4$ and to a $Re_p \approx 6.4 \cdot 10^3$. Moreover, to maximize the flow stability before the orifice, this is placed close (around 100.0 mm) to the end of the pipe in the flow direction.

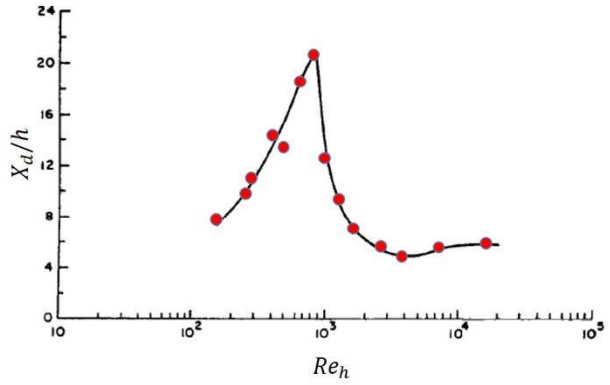

Fig. 3. Non-dimensional distance of reattachment versus Reynolds number (modified from Westphal et al, 1984 [19]).

The convergent reach is 50.0 mm long and with a wall inclination of around 20°, in order to minimize the flow separation also in this case.

The pipe of Figure 1 is immersed in a constant head tank with a volume of 2.0 m^3 (2.0 m long and with a section of 1.0 m × 1.0 m), with transparent Perspex walls (Figure 4). The transparent Perspex walls are needed in order to have an optical access to the flow and to perform non-intrusive and quasi-continuous-in-space measurements via Digital Image Analysis (DIA) techniques (a brief review on DIA techniques can be found in Ferrari, 2017 [20]). Consequently, the experimental set-up includes a high-frequency video acquisition system (with a camera placed vertically above the pipe) and a laser with a cylindrical lens, in order to obtain a horizontal light sheet. As during the experimental campaign both velocity (via Feature Tracking Velocimetry, FTV, see Besalduch et al., 2013 [21] and 2014 [22] for details) and concentration (via Laser induced Fluorescence, LIF) measurements were performed, a green laser was employed in the first case and a blue laser in the second case. In the case of FTV, the flow was seeded with non-buoyant pine pollen particles; in the case of LIF, the flow was seeded with fluorescein dye (the quantity was in the range allowing a linear relation between the dye concentration and the light intensity, Sutton et al., 2008 [23]). An example of an instantaneous LIF image is shown on Figure 5, where light green means a high concentration, pale green a low concentration and black zero concentration.

The two DIA techniques employed have been designed and developed by the Hydraulics Group of the DICAAR - University of Cagliari, and have been applied in the recent past in laboratory investigations to measure tracer concentrations (Ferrari et al., 2015 [24], Ferrari et al., 2018a [25] and 2018b [26], Badas et al. (2018) [27], Ferrari et al (2019) [28]), wave position (Ferrari et al., 2016 [29], Gallerano et al (2019) [30]), flow velocity (Querzoli, 1996 [31], Badas and Querzoli, 2011 [32], Simone et al., 2013 [33], Garau et al., 2018 [34], Badas et al. (2019) [35]) and acceleration (Ferrari et al, 2007 [36], Ferrari and Rossi, 2008 [37], Ferrari et al, 2008 [38], Lardeau et al., 2008 [39], Rossi et al, 2009 [40]). Among the engineering fields of interest, the DIA techniques have been employed in the civil and industrial field (such as in the present paper), in the environmental field (Ferrari et al., 2016 [41], Badas et al., 2017 [42], or in Garau et al., 2017 [43], Di Bernardino et al. (2017) [44], Ferrari et al., 2017 [45], Garau et al., 2018 [46], Badas et al., 2019 [47]) and biomedical fields (Badas et al., 2015 [48], Espa et al, 2012 [49], Querzoli et al (2019) [50]).

During the velocity measurements, the flow rates were computed through the velocity measurements FTV, while during the concentration measurements a flowmeter (Transonic 400-series coupled with a TS410 tubing module was employed. The flowmeter was placed downstream the convergent reach, so Q_1 was measured closing the orifice on the lateral wall of the pipe, then the orifice was opened and Q_2 was measured while the jet was flowing, and Q_3 was computed as the difference between Q_1 and Q_2. The ratio between the flow rates can be adjusted via two valves, one upstream the divergent reach and one downstream the convergent reach.

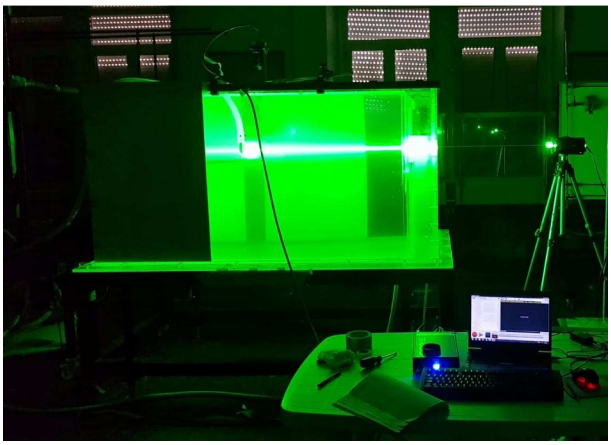

Fig. 4. Experimental setup.

As stated before, on the acquired LIF images the concentration field is proportional to the light intensity, so a quantitative measure of the concentration is allowed. Under the hypothesis of ergodicity, the mean and the variance on each pixel were obtained by time averaging over the 6000 samples recorded for each run. Then the mean concentration values were normalised with the mean value at the outlet C_0 (initial jet concentration), in order to obtain the fields of the reduction of the concentration C/C_0 (e.g., Figure 6). The fields of the variance of the concentration were normalised by the square of C_0 (Figure 10).

In order to measure the inclination of the jet, the axis of the jet itself has to be defined. As here the focus is on

the jet region close to the orifice, the jet axis was defined as the straight line passing through the jet origin that best fits, in a least-square sense, the concentration maxima on the vertical sections close to the jet origin (e.g., see Figure 6). As previously stated, the jet inclination angle θ was consequently defined as the one between the above defined jet axis and a line perpendicular to the pipe axis. On Figures from 6 to 9, the concentration maxima are highlighted with white asterisks, the jet axis with a green line and the line perpendicular to the pipe axis with a blue line.

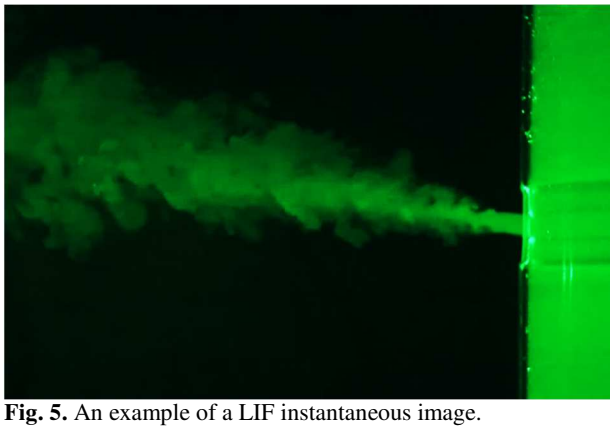

Fig. 5. An example of a LIF instantaneous image.

4 Results

In this section, some preliminary results concerning the concentration measurements via LIF will be shown. In particular, two of the measured quantities will be shown (mean and variance of the concentration), so this section is divided into two subsections.

In the first one, some of the non-dimensional mean concentration fields will be shown, in order to show the modifications induced on the jet inclination and shape by the different flow rate ratios *r*.

In the second subsection, the map of the non-dimensional variance of the concentration will be shown, in order to further highlight the lack of axisymmetry of this kind of jet when r increases.

On all the Figures from 6 to 10, the jet flows from the right to the left, the x- and y-axis are non-dimensionalized by the orifice diameter D_J and the origin of the x-axis and x-axis is placed on the centre of the orifice (jet origin).

4.1 Mean Concentration fields

The fields of the mean non-dimensional concentration C/C_0, where C_0 is the mean concentration measured at the outlet (that is the initial jet concentration), are shown in false colours from Figure 6 to Figure 9: dark red implies high concentration values (or a low dilution), dark blue implies low concentration values (or a low dilution), with increasing values of the flow rate ratio *r*, form very low values (r = 0.015, Figure 6) to higher values (r = 0.482, Figure 9).

On Figure 6, it is possible to see that when *r* is low (that is when most of the flow rate is going beyond the orifice withut passing throut it), the jet is not perpendicular to the pipe axis but, instead, there is a relevant angle θ between the jet axis and the line perpendicular to the pipe axis ($\theta \approx 27°$). Moreover, at a certain distance from the orifice, the upstream jet region (i.e. towards positive values of y/D) tends to widens more than the downstream jet region (i.e. towards negative values of y/D): this implies that the entrainment in the upstream region is higher than in the downstream region, so the upstream region experiences slowest velocities and, as a consequence, the jet tends to bend towards the positive y/D values. From another point of view, we can state that the jet has a low rigidity that tends suddenly to lose. So we can say that, for low values of *r*, the jet is not pependicular to the pipe axis and not even axysimmetric.

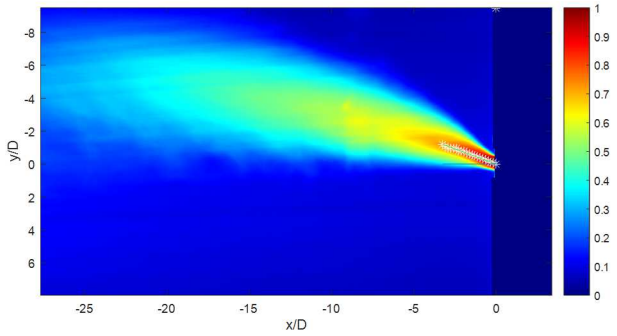

Fig. 6. Mean non-dimensional concentration C/C_0 field (C_0 is the mean concentration measured at the outlet, i.e. the initial jet concentration) for a jet with r = 0.015 ($\theta \approx 27°$); the white asterisks are the concentration maxima in the initial region of the jet, the green line is the jet axis, the blue line is the line perpendicular to the pipe axis.

Looking at Figure 7 (r = 0.053) and Figure 8 (r = 0.103), it is possible to not how, when *r* increases i.e. when more flow rate is passing through the orifice and less is going beyond it, the angle θ tends to decrease, the differencies between the upstream and downstream regions of the jet tend to reduce and the curvature is less accentuated.

On Figure 8, a jet with a higher value of *r* is shown (r = 0.482, meaning that almost half of the flow rate before the orifice becomes jet flow rate through the orifice), the initial region of the jet is almost perpendicular to the pipe axis ($\theta \approx 2°$) and almost axisymmetric.

As a consequence, we can state that, when a jet issues from an orifice in the lateral wall of pipe where a flow is moving, the jet is not perpendicular to the pipe axis but, instead, there is an angle of inclination in the downstream direction that is inversely proportional to the ratio of the jet flow rate to the pipe flow rate before the orifice *r*. The same consideration applies to the jet axisymmetry, as this tends to decrease when *r* decreases.

4.2 Concentration Variance

The field of non-dimensional variance of the concentration (normalized with the square of C_0) for a jet with r = 0.011 is shown, in false colours, on Figure 10. As the concentration variance is proportional to the turbulence intensity, high variance values (dark red)

highlight regions of intense turbulent fluctuations, low variance values (dark blue) regions of very low turbulent fluctuations.

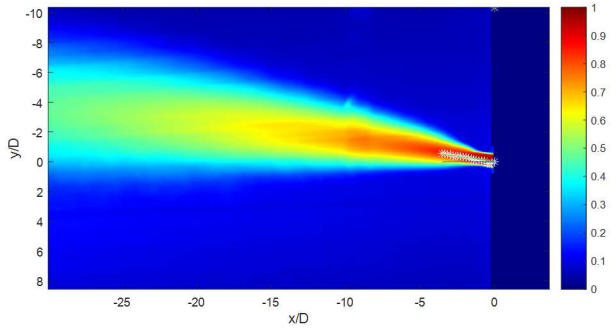

Fig. 7. Mean non-dimensional concentration C/C_0 field (C_0 is the mean concentration measured at the outlet, i.e. the initial jet concentration) for a jet with r = 0.053 ($\theta \approx 12°$); the white asterisks are the concentration maxima in the initial region of the jet, the green line is the jet axis, the blue line is the line perpendicular to the pipe axis.

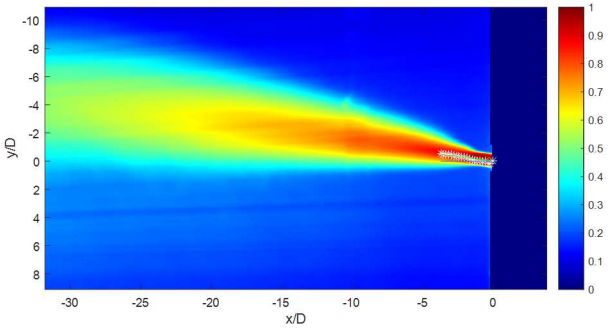

Fig. 8. Mean non-dimensional concentration C/C_0 field (C_0 is the mean concentration measured at the outlet, i.e. the initial jet concentration) for a jet with r = 0.103 ($\theta \approx 8°$); the white asterisks are the concentration maxima in the initial region of the jet, the green line is the jet axis, the blue line is the line perpendicular to the pipe axis.

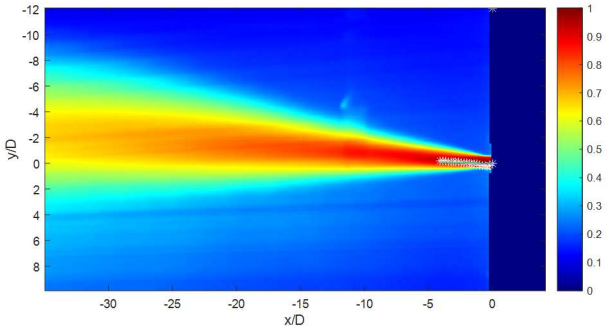

Fig. 9. Mean non-dimensional concentration C/C_0 field (C_0 is the mean concentration measured at the outlet, i.e. the initial jet concentration) for a jet with r = 0.482 ($\theta \approx 2°$); the white asterisks are the concentration maxima in the initial region of the jet, the green line is the jet axis, the blue line is the line perpendicular to the pipe axis.

This Figure highlights what stated above about the lack of axisymmetry of this kind of jets. First of all, the upstream and downstream region are different. The highest values are found in the downstream region, close to the jet origin, so the entrainment is larger on the downstream region: this could be the reason for the fact that the jet tends to initially deflect to the downstream direction. Alternatively, considering that the jet inclination is also a consequence of the flow pattern inside the pipe near the orifice, the largest variance in the upstream jet region close to the outlet could also be the consequence of this. This is currently under investigation, as we are performing the analysis on the velocity measurements also in the region inside the pipe and close to the outlet.

Even if the highest variance values are found on the downstream region, the area of high variance values on the upstream region is longer than the downstream one, giving an explanation to the reason of the second deflection of the jet, in an opposite direction.

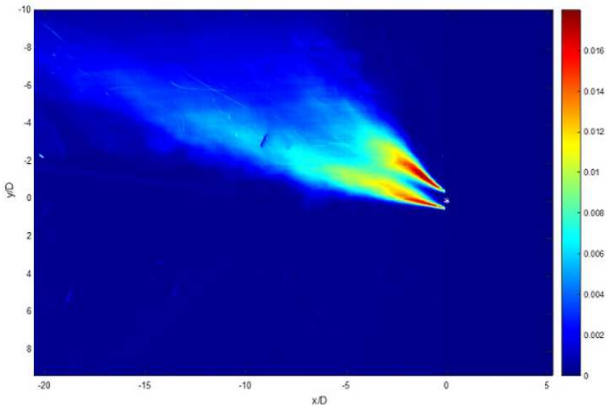

Fig. 10. Non-dimensional field of the variance of the concentration, non-dimensionalized with the square of the mean concentration measured at the outlet (highlighted by a yellow point), i.e. the initial jet concentration C_0, for a jet with r = 0.011.

5 Conclusions

In this work, we have shown some preliminary results regarding the behaviour of fluid jets released, in a receiving body of the same fluid, from a sharp-edged orifice in the lateral wall of a pipe where a certain flow rate is flowing. The concentration fields for various ratios of the jet flow rate to the pipe flow rate (r) have been measured in the Hydraulics Laboratory of the DICAAR – University of Cagliari, via a LIF technique, a non-intrusive and quasi-continuous-in-space Digital Image Analysis technique.

The preliminary results showed above highlight that the jets are not perpendicular to the pipe flow nor axisymmetric. In particular, the inclination of the jet tends to increase when r decreases. This result can have a relevant practical application, as it can be used to forecast where the jet will move once outside the orifice.

A similar consideration can be drawn regarding the jet axisymmetry, as this tends to decrease when r decreases. Moreover, the variance field seems to suggest that the different entrainments experienced from the two regions of the jet makes it bend twice, on the downstream direction soon after the release and on the upstream direction at a certain distance from the orifice.

We are currently performing and analysing velocity measurements, in order to investigate, among the others, the flow inside the pipe in the region close to the orifice, the velocity fields and the Reynolds stresses in the jet and the relation of r versus θ.

The Authors would like to acknowledge Mr. Antonio Mascia.

References

1. T. M. Missimer, B. Jones, and R. G. Maliva, *Intakes and Outfalls for Seawater Reverse-Osmosis Desalination Facilities* (Springer Berlin Heidelberg, 2015).
2. S. Ferrari and G. Querzoli, J. Hydraul. Res. **48**, 632 (2010).
3. C. Avanzini, in *Proc 4th Intl Conf Mar. Waste Water Dispos. Mar. Environ. 2nd Intl Exhib. Mater. Equip. Serv. Coast. Waste Water Treat. Plants Outfalls Sealines Antalya Turk.* (Mem Ajans, Istambul, 2006).
4. J. R. Wood, in *Ocean Dispos. Wastewater* (World Sci. Publ., Singapore, 1993), pp. 71–84.
5. W. Xue, W. Huai, Z. Qian, Z. Yang, and Y. Zeng, Eng. Comput. **31**, 1379 (2014).
6. A. S. Al-Ghamdi, J. Coast. Conserv. **14**, 63 (2010).
7. G. A. Anderson, A. Kommareddy, T. Suess, and S. P. Gent, in *ASME 2014 8th Int. Conf. Energy Sustain. ES 2014 Collocated ASME 2014 12th Int. Conf. Fuel Cell Sci. Eng. Technol.* (ASME, 2014).
8. K. Osman, S. M. N. Al Khaireed, M. K. Ariffin, and M. Y. Senawi, Energy Convers. Manag. **49**, 3270 (2008).
9. J. E. van Zyl, Procedia Eng. **89**, 273 (2014).
10. M. Soleimani nia, P. Oshkai, and N. Djilai, Int. J. Hydrog. Energy **44**, 15262 (2019).
11. M. Ferrante, C. Massari, E. Todini, B. Brunone, and S. Meniconi, J. Hydroinformatics **15**, 666 (2013).
12. R. Mohsin, Z. A. Majid, and F. L. Tan, Eng. Fail. Anal. **48**, 30 (2015).
13. A. M. Cassa, J. E. van Zyl, and R. F. Laubsher, Urban Water J. **7**, 109 (2010).
14. J. E. van Zyl and C. R. I. Clayton, Proc. Inst. Civ. Eng. Water Manag. **160**, 109 (2007).
15. M. Soleimani nia, B. Maxwell, P. Oshkai, and N. Djilali, Int. J. Hydrog. Energy **43**, 9379 (2018).
16. A. Hashiehbaf and G. P. Romano, Int. J. Heat Fluid Flow **44**, 208 (2013).
17. J. Mi, G. J. Nathan, and D. S. Nobes, J. Fluids Eng. **123**, 878 (2001).
18. J. Mi, P. Kalt, G. J. Nathan, and C. Y. Wong, Exp. Fluids **42**, 625 (2007).
19. R. V. Westphal, J. P. Johnston, and J. K. Eaton, 284 (n.d.).
20. S. Ferrari, EPJ Web Conf. **143**, 01001 (2017).
21. L. A. Besalduch, M. G. Badas, S. Ferrari, and G. Querzoli, EPJ Web Conf. **45**, 01012 (2013).
22. L. A. Besalduch, M. G. Badas, S. Ferrari, and G. Querzoli, EPJ Web Conf. **67**, 02007 (2014).
23. J. A. Sutton, B. T. Fisher, and J. W. Fleming, Exp. Fluids **45**, 869 (2008).
24. S. Ferrari and G. Querzoli, EPJ Web Conf. **92**, 02018 (2015).
25. S. Ferrari, M. Badas, and G. Querzoli, Water **10**, 726 (2018).
26. S. Ferrari, M. G. Badas, and G. Querzoli, EPJ Web Conf. **180**, 02025 (2018).
27. M. G. Badas, M. Garau, A. Seoni, S. Ferrari, and G. Querzoli, J. Phys. Conf. Ser. **1110**, 012003 (2018).
28. S. Ferrari, M. G. Badas, M. Garau, L. Salvadori, A. Seoni, and G. Querzoli, EPJ Web Conf. **213**, 02017 (2019).
29. S. Ferrari, M. G. Badas, and G. Querzoli, EPJ Web Conf. **114**, 02022 (2016).
30. F. Gallerano, G. Cannata, M. Tamburrino, S. Ferrari, M. G. Badas, and G. Querzoli, WSEAS Trans. FLUID Mech. **14**, 84 (2019).
31. G. Querzoli, Atmos. Environ. **30**, 2821 (1996).
32. M. G. Badas and G. Querzoli, Exp. Fluids **50**, 1093 (2011).
33. F. Simone, M. G. Badas, L. A. Besalduch, and Q. Giorgio, Int. Symp. Turbul. Shear Flow Phenom. TSFP 2013 (2013).
34. M. Garau, M. G. Badas, S. Ferrari, A. Seoni, and G. Querzoli, Int. J. Environ. Pollut. **65**, 103 (2019).
35. M. G. Badas, S. Ferrari, M. Garau, S. Seoni, and G. Querzoli, Bound.-Layer Meteorol. **in press**, (2019).
36. S. Ferrari, L. Rossi, and J. C. Vassilicos, in *Adv. Turbul. XI - Proc. 11th EUROMECH Eur. Turbul. Conf.* (2007), pp. 485–487.
37. S. Ferrari and L. Rossi, Exp. Fluids **44**, 873 (2008).
38. S. Ferrari, P. Kewcharoenwong, L. Rossi, and J. C. Vassilicos, in *IUTAM Symp. Flow Control MEMS*, edited by J. F. Morrison, D. M. Birch, and P. Lavoie (Springer Netherlands, Dordrecht, 2008), pp. 267–272.
39. S. Lardeau, S. Ferrari, and L. Rossi, Phys. Fluids **20**, 127101 (2008).
40. L. Rossi, S. Bocquet, S. Ferrari, J. M. Garcia de la Cruz, and S. Lardeau, Int. J. Heat Fluid Flow **30**, 505 (2009).
41. S. Ferrari, M. G. Badas, M. Garau, A. Seoni, and G. Querzoli, HARMO 2016 - 17th Int. Conf. Harmon. Atmospheric Dispers. Model. Regul. Purp. Proc. 351 (2016).
42. M. G. Badas, S. Ferrari, M. Garau, and G. Querzoli, J. Wind Eng. Ind. Aerodyn. **162**, 24 (2017).
43. M. Garau, M. G. Badas, S. Ferrari, A. Seoni, and G. Querzoli, HARMO 2017 - 18th Int. Conf. Harmon. Atmospheric Dispers. Model. Regul. Purp. Proc. 470 (2017).
44. A. D. Bernardino, P. Monti, G. Leuzzi, F. Sammartino, and S. Ferrari, in *HARMO 2017 - 18th Int. Conf. Harmon. Atmospheric Dispers. Model. Regul. Purp. Proc.* (Hungarian Meteorological Service, 2017), pp. 460–464.
45. S. Ferrari, M. G. Badas, M. Garau, A. Seoni, and G. Querzoli, Int. J. Environ. Pollut. **62**, 22 (2017).
46. M. Garau, M. G. Badas, S. Ferrari, A. Seoni, and G. Querzoli, Bound.-Layer Meteorol. **167**, 123 (2018).
47. M. G. Badas, M. Garau, G. Querzoli, L. Salvadori, and S. Ferrari, Int. J. Environ. Pollut. **in press**, (2019).
48. M. G. Badas, S. Espa, S. Fortini, and G. Querzoli, EPJ Web Conf. **92**, 02004 (2015).
49. S. Espa, M. G. Badas, S. Fortini, G. Querzoli, and A. Cenedese, Eur. J. Mech. - BFluids **35**, 9 (2012).
50. G. Querzoli, V. Satta, G. Matta, S. Ferrari, M. G. Badas, and G. Bitti, J. Phys. Conf. Ser. **1249**, 012006 (2019).